Received: 31 May 2022 | Revised: 30 October 2022 | Accepted: 11 November 2022

DOI: 10.1111/cas.15658

ORIGINAL ARTICLE

Cancer Science WILEY

Methyltransferase-like 3 promotes cervical cancer metastasis by enhancing cathepsin L mRNA stability in an N6-methyladenosine-dependent manner

Pingping Liu[1] | Mingxiu Ju[1] | Xiaojing Zheng[1] | Yinan Jiang[1] | Xingjuan Yu[2] | Baoyue Pan[1] | Rongzhen Luo[3] | Weihua Jia[4] | Min Zheng[1]

[1]Department of Gynecology, Sun Yat-Sen University Cancer Center, State Key Laboratory of Oncology in South China, Collaborative Innovation Center for Cancer Medicine, Guangzhou, China

[2]Department of Hepatobiliary Oncology, Collaborative Innovation Center for Cancer Medicine, State Key Laboratory of Oncology in South China, Sun Yat-Sen University Cancer Center, Guangzhou, China

[3]Department of Pathology, Sun Yat-Sen University Cancer Center, State Key Laboratory of Oncology in South China, Collaborative Innovation Center for Cancer Medicine, Guangzhou, China

[4]Biobank of Sun Yat-Sen University Cancer Center, State Key Laboratory of Oncology in South China, Collaborative Innovation Center for Cancer Medicine, Guangzhou, China

Correspondence
Min Zheng, Department of Gynecology, Sun Yat-Sen University Cancer Center, State Key Laboratory of Oncology in South China, Collaborative Innovation Center for Cancer Medicine, 651 Dongfeng Road East, Guangzhou, Guangdong 510060, China.
Email: zhengmin@sysucc.org.cn

Funding information
the Natural Science Foundation of China, Grant/Award Number: grant number 81872434

Abstract

N6-methyladenosine (m6A) is a highly abundant RNA modification in eukaryotic cells. Methyltransferase-like 3 (METTL3), a major protein in the m6A methyltransferase complex, plays important roles in many malignancies, but its role in cervical cancer metastasis remains uncertain. Here, we found that METTL3 was significantly upregulated in cervical cancer tissue, and its upregulation was associated with a poor prognosis in cervical cancer patients. Knockdown of METTL3 significantly reduced cervical cancer cell migration and invasion. Conversely, METTL3 overexpression markedly promoted cervical cancer cell metastasis in vitro and in vivo. Furthermore, METTL3 mediated the m6A modification of cathepsin L (*CTSL*) mRNA at the 5′-UTR, and the m6A reader protein insulin-like growth factor 2 mRNA-binding protein 2 (IGF2BP2) bound to the m6A sites and enhanced *CTSL* mRNA stability. Our results indicated that METTL3 enhanced *CTSL* mRNA stability through an m6A-IGF2BP2-dependent mechanism, thereby promoting cervical cancer cell metastasis. These findings provide insights into a novel m6A modification pattern involved in cervical cancer development.

KEYWORDS
cervical cancer, CTSL, m6A, metastasis, METTL3

1 | INTRODUCTION

Cervical cancer is the most common malignancy of the female reproductive system and has the highest morbidity and mortality rates of all gynecological tumors in China.[1,2] Despite the increased implementation of screening and prevention strategies, the occurrence of cervical cancer has increased, and the median age of patients has decreased, highlighting the serious threat it poses to women's health. The main treatment methods for cervical cancer are surgery and radiotherapy. Although standardized treatment cures some patients, some experience tumor recurrence and metastasis, which are the main causes of cancer treatment failure and are difficult clinical problems for cervical cancer patients. Thus, understanding the molecular mechanism associated with cervical cancer metastasis will be beneficial to the clinical management of these patients.[3–5]

The N6-methyladenosine (m6A) modification involves methylation at the sixth-position nitrogen of adenine.[6] m6A methylation occurs in mRNA and transfer, ribosomal, and noncoding RNA.[7,8] The m6A modification is catalyzed by methyltransferases ("writers"), reversed by demethylases ("erasers"), and recognized by binding proteins ("readers").[9,10] Abnormal m6A modifications caused by m6A modification-related enzymes is closely associated with human disease, especially cancers.[11,12] Methyltransferase-like 3 (METTL3) is a key protein in the m6A methyltransferase complex, but its reported roles in tumor progression differ between cancer types. For instance, METTL3 plays an oncogenic role in leukemia,[13,14] hepatoma,[15,16] bladder cancer,[17–19] and colorectal carcinoma,[20] but an antioncogenic role in glioblastoma and endometrial cancers.[21–23] Recent studies have shown that METTL3 promotes cervical cancer proliferation and the Warburg effect through YTH N6-methyladenosine RNA-binding protein 1 (YTHDF1)/hexokinase 2 modification.[24] However, the functions and associated molecular mechanisms of METTL3 in cervical cancer remain poorly understood. Thus, we sought to determine whether METTL3 modulates cervical cancer metastasis.

We found that METTL3 expression was upregulated in cervical cancer tissue and higher METTL3 expression levels were associated with a worse prognosis in cervical cancer patients. Moreover, METTL3 promoted tumor metastasis in vitro and in vivo by increasing the expression level of its downstream target gene, cathepsin L (*CTSL*). METTL3 increased the m6A levels of *CTSL* transcripts, thus increasing their stability. Overall, our results indicated that METTL3 is a predictor of cervical cancer metastasis and illustrated a new epigenetic mechanism through which METTL3 promotes cervical cancer metastasis.

2 | MATERIALS AND METHODS

2.1 | Clinical samples

Paraffin-embedded tissues from 129 patients with stage IB1-IIA2 (FIGO 2009 stage version) cervical squamous cell carcinoma (CSCC) who underwent surgical resection and 75 paraffin-embedded normal cervical epithelial tissue specimens (including uterine fibroids and normal tumor-adjacent cervical epithelial tissue from patients with cervical carcinoma in situ or early-stage cervical cancer [stage IA-IIA]) were collected from the Sun Yat-sen University Cancer Center. Approximately 30 fresh tissue samples from CSCC patients and those with a normal cervical epithelium were collected separately and stored in RNA-later (Thermo Fisher Scientific) for subsequent RT-quantitative PCR (qPCR) analysis. The patients' clinicopathologic information was retrieved retrospectively from electronic medical records. This study followed the ethical standards of the Declaration of Helsinki and was approved by the Institutional Review Board and Independent Ethics Committee of Sun Yat-sen University Cancer Center (B2021-384-01).

2.2 | Cell culture

The human cervical cancer cell lines CaSki and SiHa, and the human kidney cell line 293FT, were purchased from the Cell Bank of the Shanghai Institutes for Biological Sciences. Normal cervical epithelial cells (NCECs) were isolated from fresh cervical epithelial tissues and cultured.[25] CaSki cells were grown in RPMI-1640 medium with 10% FBS (HyClone). SiHa and 293FT cells were cultured in DMEM with 10% FBS, and NCECs were cultured in Keratinocyte-SFM medium (Gibco BRL) with 10% FBS. All cells were grown in an incubator at 37°C and 5% CO_2. The cells were authenticated by Guangzhou Cellcook Biotech Co., Ltd. before use.

2.3 | Immunohistochemistry

Briefly, tissues were dewaxed in xylene and then hydrated. Endogenous peroxidase activity was blocked by 0.3% H_2O_2 treatment for 10 min. Antigen retrieval was carried out by heating (120°C) the sections in EDTA (PH 9.0) for 10 min. The sections were then incubated with primary Abs against METTL3 (1:500 dilution; ab195352; Abcam) or CTSL (1:200 dilution; 10,938-1-AP; Proteintech) at 4°C overnight, followed by incubation with a secondary Ab. The results were developed with 3,3′-diaminobenzidine tetrahydrochloride (Dako).

The METTL3 and CTSL immunostaining scores were calculated based on staining intensity and the percentage of positively stained cells. Intensity scores were assigned based on negative (0), weak (1), moderate (2), and strong (3) staining. Positive staining scores were assigned as follows: 0, <5% positivity; 1, 5%–24% positivity; 2, 25%–49% positivity; 3, 50%–74% positivity; and 4, 75%–100% positivity. The final score was calculated by multiplying the intensity score by the positive staining score. Two pathologists evaluated all specimens in a blinded manner. The median immunohistochemistry (IHC) score was considered as the optimal METTL3 cut-off value.

2.4 | Reverse transcription-qPCR

Total RNA was extracted from cells and tissues using TRIzol (Life Technologies) according to the manufacturer's protocol. Reverse transcription reactions were carried out using the GoScript Reverse Transcription Mix and random primers (Promega) according to the manufacturer's instructions. Polymerase chain reaction was undertaken using GoTaq qPCR Master Mix (Promega). Relative mRNA expression levels were determined using the $2^{(-\Delta\Delta CT)}$ method. The primer sequences are listed in Table S1. β-Actin was used as the internal control.

2.5 | Western blot analysis

Proteins were lysed in radioimmunoprecipitation assay buffer containing protease inhibitors (Beyotime Biotechnology), separated by electrophoresis and transferred to PVDF membranes (Bio-Rad). After overnight incubation with primary Abs (anti-METTL3 [1:1000 dilution, ab195352; Abcam], anti-CTSL [1:500 dilution, 66,914-1-Ig; Proteintech], anti-insulin-like growth factor 2 mRNA-binding protein [IGF2BP2] [1:1000 dilution, ab128175; Abcam], anti-METTL14 [1:1000 dilution, ab220030' Abcam], anti-RNA binding motif protein 15 [RBM15] [1:1000 dilution; PTM-6163; Jingjie PTM BioLab], and anti-β-actin [1:5000 dilution; 4970S; Cell Signaling Technology]), the membranes were incubated with a HRP-conjugated secondary Ab (1:5000 dilution, 7076S, 7074S; Cell Signaling Technology). The immunoreactions were visualized using the ECL Plus substrate (Merck Millipore). β-Actin was used for normalization.

2.6 | Transfection and plasmid construction

Short interfering RNAs targeting *METTL3*, *CTSL*, *IGF2BP2*, *METTL14*, and *RBM15* mRNAs, and a negative control siRNA, were designed by RiboBio. Co, Ltd. The siRNA sequences are listed in Table S2. Short interfering RNA transfection was achieved using Lipofectamine 3000 (Invitrogen) following the manufacturer's instructions. A plasmid directing *METTL3* overexpression (Guangzhou FulenGen Co, Ltd.) was transfected into 293FT cells to produce lentivirus vectors. The cells were then infected with the lentivirus in the presence of polybrene and selected for 1 week with 2–4 μg/ml puromycin. Plasmids for *CTSL* and *CTSL* with WT or mutant m6A region were purchased from Guangzhou Da Hong.

2.7 | Cell migration assays

Wound healing assays were carried out in 6-well plates. After incubation for 24 h at 37°C with 5% CO_2, a scratch was made using a 200 μl pipette tip. The cells were then washed three times with PBS and cultured in FBS-free medium. Cell migration was recorded at 0, 24, and 36 h under the microscope. The migration distance was calculated using ImageJ software (NIH).

Transwell migration assays were undertaken using 24-well plate inserts with an 8 μm pore size (Corning). The upper chamber was seeded with 0.5×10^5 (SiHa) or 1×10^5 (CaSki) cells/well in 200 μl serum-free medium. The lower chamber was filled with 500 μl culture medium containing 10% FBS. After incubation for approximately 6 (SiHa cells) or 18 (CaSki cells) h at 37°C in 5% CO_2, the chambers were fixed with 4% paraformaldehyde for 20 min and stained with 0.1% crystal violet for 20 min at room temperature. The migrated cells were counted under a microscope.

2.8 | Cell invasion assays

Transwell invasion assays were carried out using 24-well plate inserts with an 8 μm pore size (Corning). The upper chambers were precoated with Matrigel (Corning) and 1×10^5 SiHa cells or 2×10^5 CaSki cells in 200 μl serum-free medium were seeded in the upper chambers. The lower chamber was filled with 500 μl culture medium containing 10% FBS. After incubation for approximately 12 (SiHa cells) or 30 (CaSki cells) h at 37°C in 5% CO_2, the chambers were fixed with 4% paraformaldehyde for 20 min, stained with 0.1% crystal violet for 20 min at room temperature, and the invading cells were counted under a microscope.

2.9 | RNA stability assay

Cells were seeded into 6-well plates, treated with actinomycin D (Act D; 10 μg/ml; APExBIO),[26] and collected after 0, 3, and 6 h. *CTSL* mRNA levels were determined by RT-qPCR, as described above. The cycle threshold (Ct) value was calculated as ΔCt = (average Ct of each time point − average Ct of t_0). The mRNA abundance was calculated as $2^{(-\Delta CT)}$ for each time point and plotted relative to the t_0 value using Prism (GraphPad).[26]

2.10 | RNA immunoprecipitation assay/methylated RNA immunoprecipitation qPCR

RNA immunoprecipitation assay (RIP)/methylated RNA immunoprecipitation (MeRIP)-qPCR was carried out using the Magna RIP RNA-Binding Protein Immunoprecipitation Kit (#17–700; Millipore Sigma) according to the manufacturer's instructions. Anti-METTL3 (ab195352; Abcam), anti-IGF2BP1 (ab184305; Abcam), anti-IGF2BP2 (11601-1-AP; Proteintech), anti-IGF2BP3 (14642-1-AP; Proteintech), anti-m6A (202,003; Synaptic Systems), and rabbit IgG control Abs were used. *CTSL* mRNA levels were quantified by RT-qPCR, with normalization to the amount of input RNA. The specificity of RNA–protein interactions was tested by IgG.

2.11 | RNA pulldown assay

We used 1 ml NP40 with protease and RNase inhibitors (Beyotime Biotechnology) to lyse cells in 10 cm dishes. Then 50 pmol of negative control, WT, or mutant probes targeting the m6A region of *CTSL* mRNA (Umine Biotechnology Co., Ltd.; Table S3) and 30 μl of streptomycin-conjugated magnetic beads (Ginbio) were combined and incubated at 4°C for 5 h. The magnetic beads were added to the cell lysis solution, and the samples were incubated overnight at 4°C. The magnetic beads were then washed six times with NP40, and 50 μl of 1× loading buffer was used to elute the protein. The results were detected by western blotting as described above.

2.12 | Animal experiments

Female BALB/c nude mice (4–5 weeks old) were purchased from the Center of Experimental Animals of Guangdong. To establish a tail vein metastasis model, 2×10^6 SiHa cells in 200 μl PBS were injected into the tail vein of each mouse ($n = 6$ for both METTL3-overexpressing and empty vector groups). The mice were killed at approximately 8 weeks, and lung tissues were isolated and embedded in paraffin. Hematoxylin and eosin staining was then used to determine the number of lung metastasis nodules. To establish the popliteal lymph node metastasis model, 1×10^6 SiHa cells in 50 μl PBS were injected subcutaneously into the footpad of each mouse ($n = 6$ for both groups). Cells from the experimental and control groups were inoculated under the right and left footpads of each mouse, respectively. After 8 weeks, the popliteal lymph nodes were excised. Metastasis-positive lymph nodes were detected by immunostaining with anti-cytokeratin Abs, and the size of the popliteal lymph nodes was calculated using the formula: $V = 1/2$ (length × width^2). Animal experiments were carried out according to the protocol approved by our institutional animal care committee (L102042021010C).

2.13 | Statistical analysis

Data from cell and animal experiments were analyzed using Prism 8.0. Analysis of variance, two-tailed Student's *t*-tests, and Pearson's χ^2-tests were used. SPSS version 22.0 (IBM Corp.) was used for clinical data analysis. Pearson's χ^2-test was used to assess the association between METTL3 levels and patients' clinicopathologic characteristics. Survival curves were plotted using the Kaplan–Meier method and compared using the log-rank test. Cox proportional hazards regression analysis was used to identify independent prognostic factors. $p < 0.05$ was used to indicate statistical significance, and all *p* values were based on two-sided test results.

3 | RESULTS

3.1 | METTL3 expression levels increased in cervical cancer tissue, and higher levels were associated with a poorer prognosis

The m6A modification, catalyzed by methyltransferases, plays an important role in regulating tumorigenesis. The most commonly studied methyltransferases include METTL3, METTL14, WTAP, KIAA1492, and RBM15.[27] We determined the mRNA levels of these methyltransferases in cervical cancer tissues and normal cervical epithelial tissues by RT-qPCR and found that only *METTL3* and *METTL14* were significantly upregulated in cervical cancer tissues (Figure 1A). To explore the role of METTL3 in cervical cancer, we used the online tools Kaplan–Meier Plotter and Gene Expression Profiling Interactive Analysis (GEPIA) for survival analyses. Patients with higher *METTL3* mRNA levels had a shorter disease-free survival time (Figure 1B). To confirm the relationship between METTL3 and cervical cancer progression, we undertook IHC staining of METTL3 in 129 cervical cancer tissues and 75 normal cervical epithelial tissues from Sun Yat-sen University Cancer Center. METTL3 levels were significantly upregulated in cervical cancer tissues (Figure 1C). METTL3 was mainly localized in the nuclei of cervical cancer cells (Figure 1D). METTL3 immunostaining scores were calculated based on staining intensity and the percentage of positively stained cells (Figure 1E). We found that higher METTL3 expression levels were associated with significantly poorer prognoses (Figure 1F,G). Additional multivariate analysis indicated that METTL3 was as an independent predictor of overall and progression-free survival in CSCC patients (Tables 1 and 2). The associations between METTL3 levels and patients' clinicopathological characteristics are presented in Table 3. Higher METTL3 expression levels were significantly associated with higher paracervical and cervical canal invasion rates (0% vs. 6.6%, $p = 0.032$; 57.4% vs. 77%, $p = 0.018$, respectively). Patients with higher METTL3 expression levels were more likely to have distant metastasis, tumor recurrence, and death Table 3.

FIGURE 1 Methyltransferase-like 3 (METTL3) is upregulated in cervical cancer tissues, which is associated with poor clinical prognosis. (A) RT-quantitative PCR analysis of *METTL3*, *METTL14*, *KIAA1492*, *RBM15*, and *WTAP* expression in cervical cancer (T) and normal cervical epithelial (N) tissues. (B) Disease-free survival based on METTL3 expression levels in cervical cancer patients, analyzed using the Kaplan–Meier Plotter and Gene Expression Profiling Interactive Analysis (GEPIA). (C) METTL3 immunohistochemistry (IHC) scores in cervical cancer and normal cervical epithelial tissues. (D,E) Representative IHC images and IHC scoring criteria. Scale bar, 100 μm. (F,G) Kaplan–Meier analysis of overall and progression-free survival in cervical cancer patients. $^*p < 0.05$, $^{**}p < 0.01$, $^{***}p < 0.001$, $^{****}p < 0.0001$

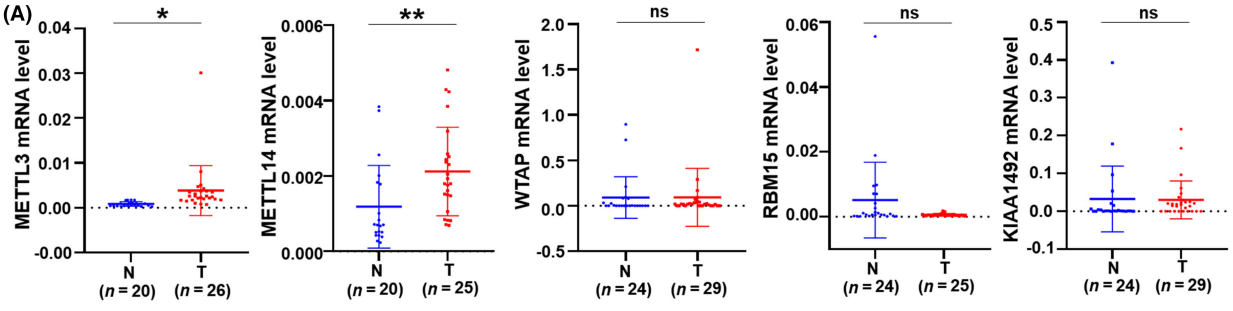

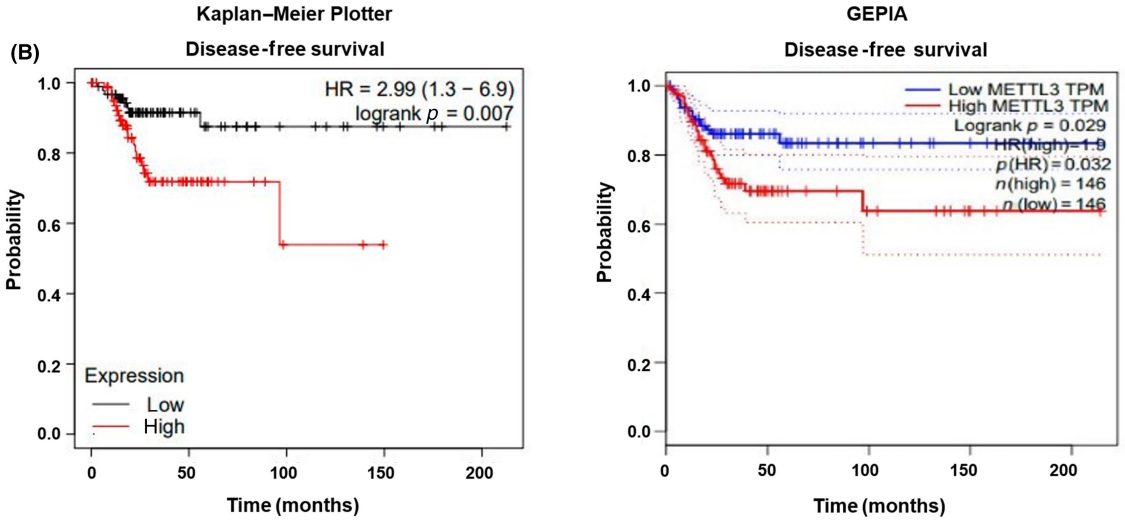

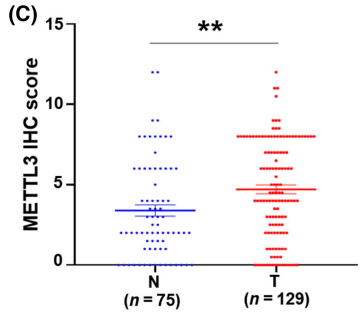

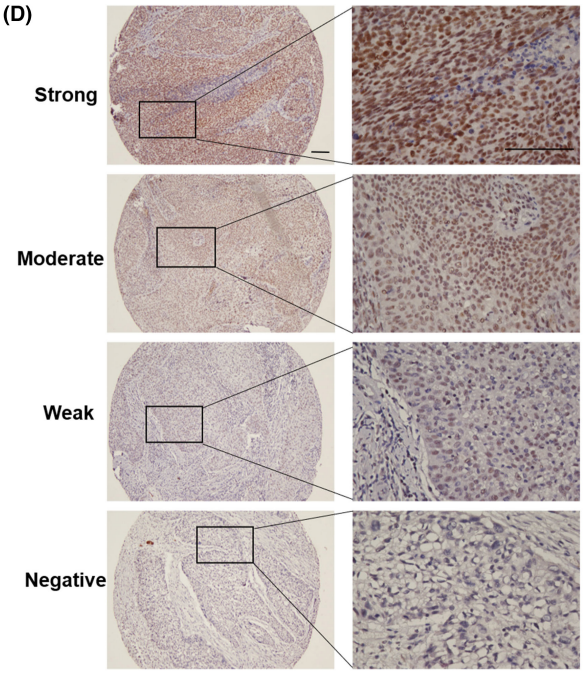

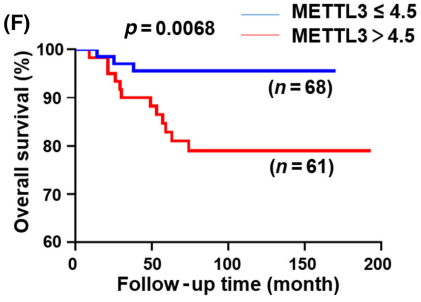

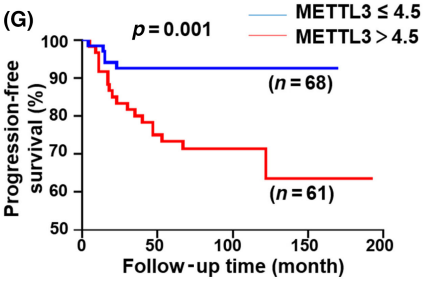

(E)

Immunohistochemical scoring criteria

Score	0	1	2	3	4
Staining intensity	Negative	Weak	Moderate	Strong	
Percentage of positive staining cells	< 5%	5%–24%	25%–49%	50%–74%	75%–100%

Note: The immunostaining score was calculated by multiplying the intensity score with the positive staining score (The highest score was 12).

TABLE 1 Univariate and multivariate analyses of prognostic factors for overall survival in patients with cervical squamous cell carcinoma

	Univariate		Multivariate	
Variable	***p* value**	**HR (95% CI)**	***p* value**	**HR (95% CI)**
Age (≤46 vs. >46 years)	0.116	2.367 (0.809–6.925)		
Tumor size (≤3.5 vs. >3.5 cm)	0.679	1.239 (0.449–3.418)		
FIGO stage (I vs. II)	**0.028**	3.127 (1.134–8.628)	0.067	2.601 (0.935–7.235)
Lymph node metastasis (positive vs. negative)	0.846	1.120 (0.356–3.522)		
Depth of cervical muscle infiltration (negative/shallow muscle layer vs. middle/deep muscle layer)	0.083	3.066 (0.864–10.875)		
Paracervical infiltration (yes vs. no)	0.250	3.341 (0.428–26.096)		
Vaginal stump positive (yes vs. no)	0.981	0.982 (0.221–4.353)		
Cervical canal invasion (yes vs. no)	0.213	2.234 (0.630–7.920)		
Lymphovascular invasion (yes vs. no)	**0.040**	3.086 (1.051–9.062)	0.120	2.375 (0.798–7.071)
Histological grade (G1–G2 vs. G3)	0.764	1.179 (0.403–3.449)		
METTL3 (≤4.5 vs. >4.5)	**0.015**	4.847 (1.367–17.183)	**0.039**	3.886 (1.073–14.074)

Note: Indicators that are not meaningful in univariate analysis are not included in multivariate analysis. Bold values indicate $p \leq 0.05$.

Abbreviations: CI, confidence interval; FIGO, International Federation of Gynecology and Obstetrics; HR, hazard ratio; METTL3, methyltransferase-like 3.

TABLE 2 Univariate and multivariate analyses of prognostic factors for progression-free survival in patients with cervical squamous cell carcinoma

	Univariate		Multivariate	
Variable	***p* value**	**HR (95% CI)**	***p* value**	**HR (95% CI)**
Age (≤46 vs. >46 years)	0.361	1.445 (0.656–3.185)		
Tumor size (≤3.5 vs. >3.5 cm)	0.534	1.283 (0.585–2.812)		
FIGO stage (I vs. II)	0.057	2.156 (0.997–4.756)		
Lymph node metastasis (positive vs. negative)	0.115	1.906 (0.855–4.246)		
Depth of cervical muscle infiltration (negative/shallow muscle layer vs. middle/deep muscle layer)	**0.010**	4.096 (1.405–11.944)	**0.032**	3.381 (1.112–10.283)
Paracervical infiltration (yes vs. no)	**0.009**	5.094 (1.505–17.248)	0.344	1.878 (0.509–6.922)
Vaginal stump positive (yes vs. no)	0.783	1.163 (0.399–3.388)		
Cervical canal invasion (yes vs. no)	**0.015**	4.471 (1.331–15.016)	0.185	2.381 (0.659–8.600)
Lymphovascular invasion (yes vs. no)	**0.041**	2.495 (1.037–6.003)	0.702	1.202 (0.468–3.083)
Histological grade (G1–G2 vs. G3)	0.947	1.028 (0.454–2.327)		
METTL3 (≤4.5 vs. >4.5)	**0.003**	4.058 (1.612–10.215)	**0.016**	3.301 (1.253–8.698)

Note: Indicators that are not meaningful in univariate analysis are not included in multivariate analysis. Bold values indicate $p \leq 0.05$.

Abbreviations: CI, confidence interval; FIGO, International Federation of Gynecology and Obstetrics; HR, hazard ratio; METTL3, methyltransferase-like 3.

3.2 | METTL3 is required for cervical cancer cell migration and invasion

To investigate the relationship between METTL3 levels and metastasis-related phenotypes, we knocked down METTL3 in CaSki and SiHa cells and constructed a SiHa cell line stably overexpressing METTL3. The altered expression levels were verified by western blotting and RT-qPCR (Figure 2A,B). Transwell cell migration and wound healing assays showed that METTL3 knockdown significantly reduced cervical cancer cell migration (Figure 2C,D,G,H), whereas METTL3 overexpression enhanced cell migration (Figure 2E,F,I,J). Cell invasion was also positively correlated with METTL3 expression levels (Figure 2K–N). We reached the same conclusion after treating cells with a METTL3 inhibitor (Figure 2O–R). Overall, our in vitro experiments demonstrated the critical role of METTL3 in cervical cancer cell migration and invasion.

TABLE 3 Clinical characteristics of 129 patients with cervical squamous cell carcinoma according to pretreatment methyltransferase-like 3 (METTL3) levels

Characteristic	Patients	METTL3 ≤ 4.5 ($n = 68$)	METTL3 > 4.5 ($n = 61$)	p value
Age (years)				
≤46	68 (52.7)	36 (52.9)	32 (52.5)	0.956
>46	61 (47.3)	32 (47.1)	29 (47.5)	
Tumor size (cm)				
≤3.5	74 (57.4)	43 (63.2)	31 (50.8)	0.155
>3.5	55 (42.6)	25 (36.8)	30 (49.2)	
FIGO stage				
I	92 (71.3)	52 (76.5)	40 (65.6)	0.172
II	37 (28.7)	16 (23.5)	21 (34.4)	
Lymph node metastasis				
Positive	34 (26.4)	14 (20.6)	20 (32.8)	0.116
Negative	95 (73.6)	54 (79.4)	41 (67.2)	
Depth of cervical muscle infiltration				
Negative/shallow muscle layer	52 (40.3)	26 (38.2)	26 (42.6)	0.612
Middle/deep muscle layer	77 (59.7)	42 (61.8)	35 (57.4)	
Paracervical infiltration				
Yes	4 (3.1)	0 (0.0)	4 (6.6)	**0.032**
No	125 (96.9)	68 (100.0)	57 (93.4)	
Vaginal stump positive				
Yes	18 (14.0)	11 (16.2)	7 (11.5)	0.442
No	111 (86.0)	57 (83.8)	54 (88.5)	
Cervical canal invasion				
Yes	86 (66.7)	39 (57.4)	47 (77)	**0.018**
No	43 (33.3)	29 (42.6)	14 (23)	
Lymphovascular invasion				
Yes	20 (15.5)	7 (10.3)	13 (21.3)	0.084
No	109 (84.5)	61 (89.7)	48 (78.7)	
Histological grade				
G1–G2	48 (37.2)	28 (41.2)	20 (32.8)	0.325
G3	81 (62.8)	40 (58.8)	41 (67.2)	
Survival status				
Survival	114 (88.4)	65 (95.6)	49 (80.3)	**0.007**
Death	15 (11.6)	3 (4.4)	12 (19.7)	
Relapse or metastasis				
Yes	25 (19.4)	6 (8.8)	19 (31.1)	**0.001**
No	104 (80.6)	62 (91.2)	42 (68.9)	

Note: Data are shown as *n* (%). Bold values indicate $p \leq 0.05$.

Abbreviation: FIGO, International Federation of Gynecology and Obstetrics.

3.3 | METTL3 promotes cervical cancer cell metastasis in vivo

To further investigate the effect of METTL3 expression levels on tumor metastasis in vivo, we constructed two metastasis models using SiHa cells. In the tail vein metastasis model, compared to treatment with the empty vector (SiHa-EV), METTL3 overexpression (SiHa-METTL3) increased distant metastasis (Figure 3A) and the number of pulmonary metastatic nodules (Figure 3B). We also used a popliteal lymph node metastasis model to investigate the effect of METTL3 on lymph node metastasis. SiHa-EV and SiHa-METTL3 cells were injected into the left and right footpads, respectively, of nude mice ($n = 6$/group), and the mice were killed at approximately 8 weeks. The volume of the popliteal lymph nodes was larger in the METTL3 overexpression group

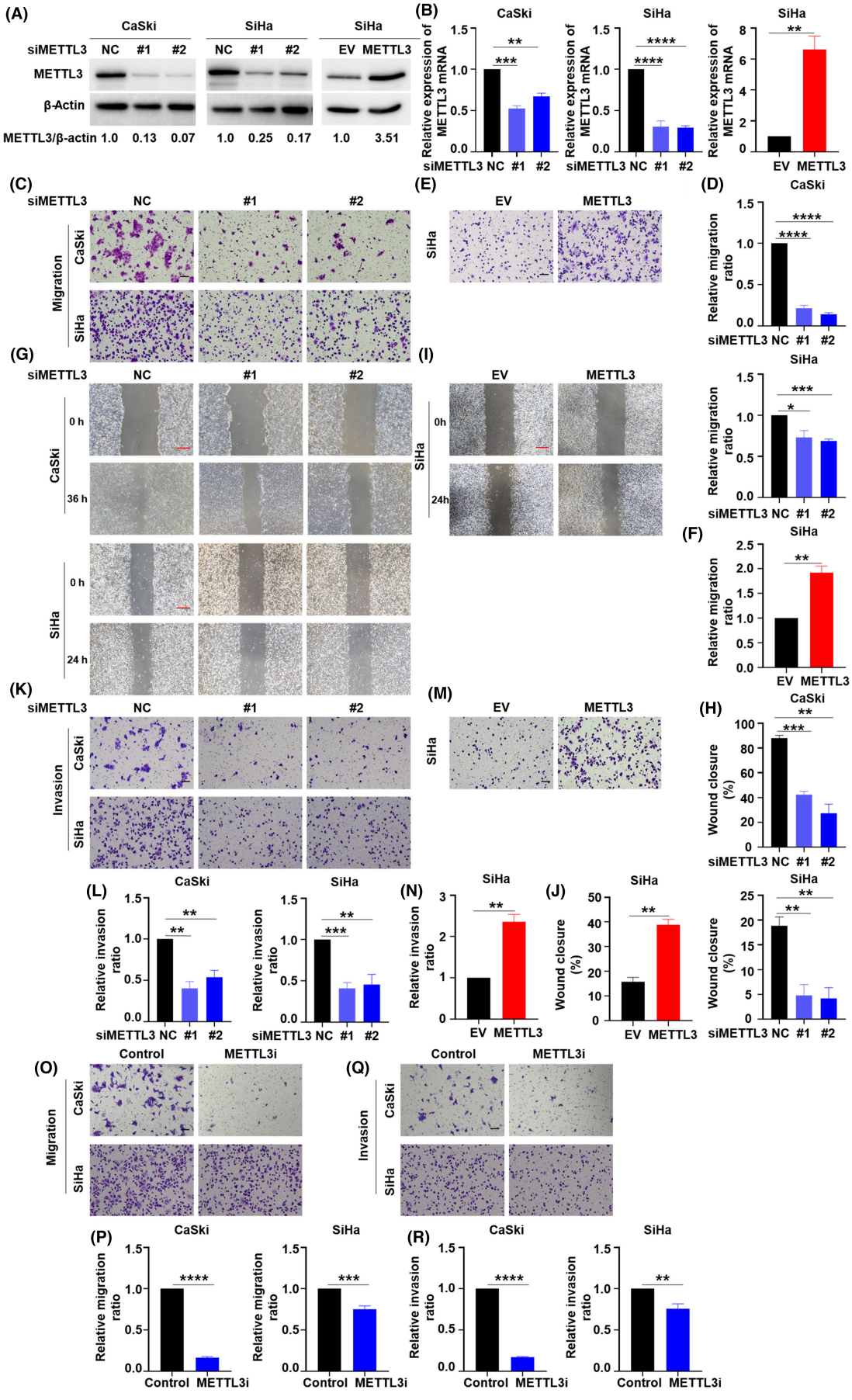
(A)
CaSki
SiHa
SiHa
siMETTL3 NC #1 #2 NC #1 #2 EV METTL3
METTL3
β-Actin
METTL3/β-actin 1.0 0.13 0.07 1.0 0.25 0.17 1.0 3.51
(B)
CaSki
SiHa
SiHa
Relative expression of METTL3 mRNA
siMETTL3 NC #1 #2
EV METTL3
(C)
siMETTL3 NC #1 #2
Migration
CaSki
SiHa
(E)
EV METTL3
SiHa
(D)
CaSki
Relative migration ratio
siMETTL3 NC #1 #2
(G)
siMETTL3 NC #1 #2
CaSki
0 h
36 h
SiHa
0 h
24 h
(I)
EV METTL3
SiHa
0h
24h
SiHa
Relative migration ratio
siMETTL3 NC #1 #2
(F)
SiHa
Relative migration ratio
EV METTL3
(K)
siMETTL3 NC #1 #2
Invasion
CaSki
SiHa
(M)
EV METTL3
SiHa
(H)
CaSki
Wound closure (%)
siMETTL3 NC #1 #2
(L)
CaSki
SiHa
Relative invasion ratio
siMETTL3 NC #1 #2
(N)
SiHa
Relative invasion ratio
EV METTL3
(J)
SiHa
Wound closure (%)
EV METTL3
SiHa
Wound closure (%)
siMETTL3 NC #1 #2
(O)
Control METTL3i
Migration
CaSki
SiHa
(Q)
Control METTL3i
Invasion
CaSki
SiHa
(P)
CaSki
SiHa
Relative migration ratio
Control METTL3i
(R)
CaSki
SiHa
Relative invasion ratio
Control METTL3i

FIGURE 2 Methyltransferase-like 3 (METTL3) promotes cervical cancer cell migration and invasion in vitro. (A) Western blot analysis of cervical cancer cells transfected with normal control (siNC), METTL3-targeted (siMETTL3#1, siMETTL3#2) siRNAs, and empty vector (EV), or METTL3-overexpression (METTL3) vector. (B) RT-quantitative PCR analysis of knockdown and overexpression efficiency. (C–F) Images and quantification of Transwell migration assays of METTL3-knockdown and -overexpressing cells. Scale bar, 100 μm. (G–J) Images and quantification of wound healing assays of METTL3-knockdown and -overexpressing cells. The average spacing of scratches at 0 and 36 h and 0 and 24 h was compared. Scale bar, 100 μm. (K–N) Images and quantification of Transwell invasion assays of METTL3-knockdown and -overexpressing cells. Scale bar, 100 μm. (O–R) Images and quantification of migration (right) and invasion (left) assays of CaSki and SiHa cells treated with an METTL3 inhibitor (METTL3i) for 48 h (10 μM, STM2457, HY-134836, MCE). Scale bar, 100 μm. $^{*}p<0.05$, $^{**}p<0.01$, $^{***}p<0.001$, $^{****}p<0.0001$

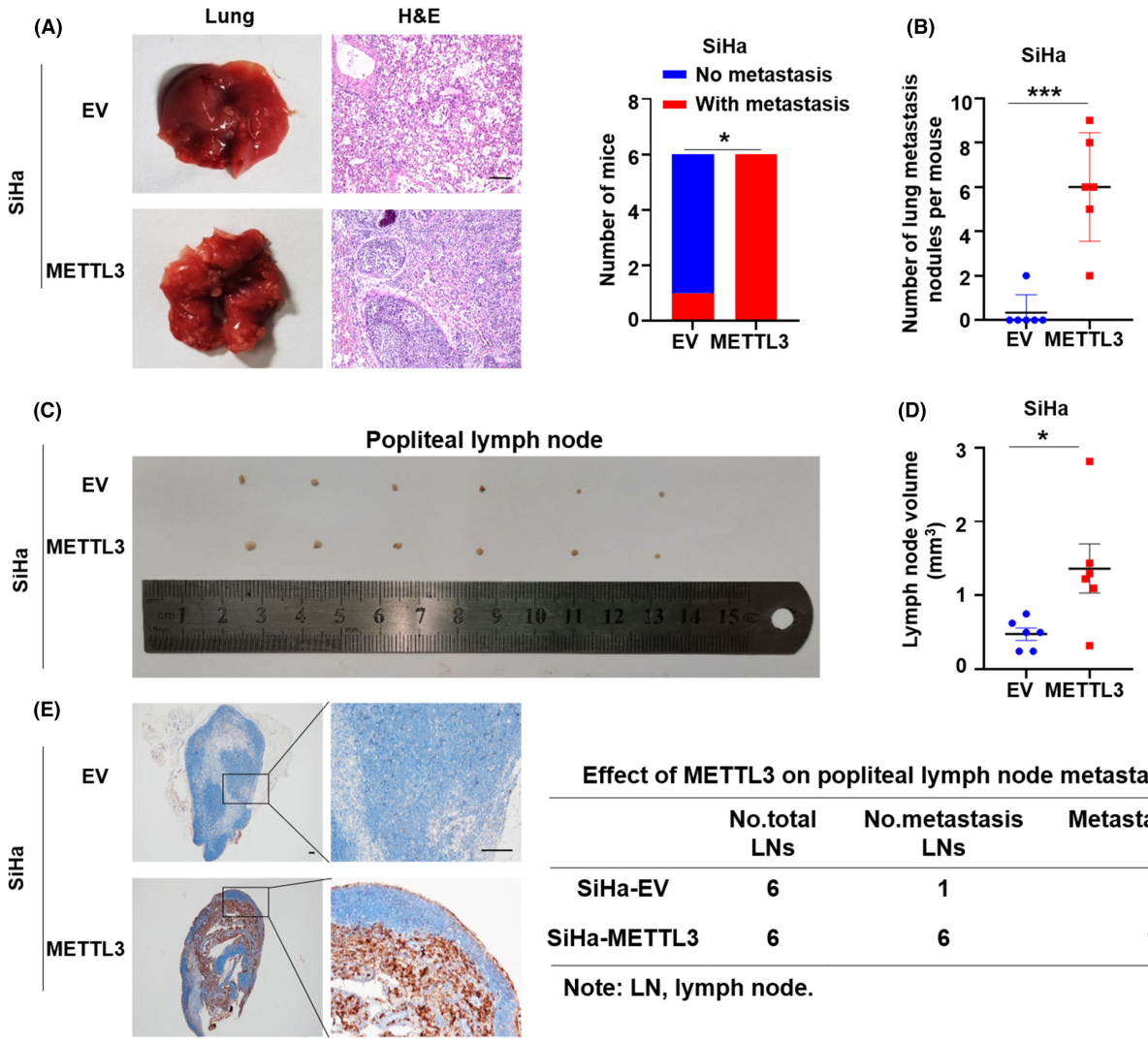

Effect of METTL3 on popliteal lymph node metastasis in vivo

	No.total LNs	No.metastasis LNs	Metastatic ratio (%)
SiHa-EV	6	1	17%
SiHa-METTL3	6	6	100%

Note: LN, lymph node.

FIGURE 3 Methyltransferase-like 3 (METTL3) inhibits cervical cancer cell metastasis in vivo. (A,B) SiHa cells with stable METTL3 overexpression and control SiHa cells transfected with an empty vector (EV) were injected into the tail vein of nude mice, and the mice were killed 8 weeks later. Lungs were dissected, embedded in paraffin, and sectioned for H&E staining. The number of lung metastasis nodules was determined. Scale bar, 100 μm. (C–E) METTL3-overexpressing and control SiHa cells were injected subcutaneously into the left and right footpads, respectively, of nude mice ($n = 6$/group), and the mice were killed 8 weeks later. Popliteal lymph nodes were removed and paraffin-embedded tissue sections were prepared. The volume of the popliteal lymph nodes was compared between the METTL3 and EV groups. Immunohistochemistry staining was carried out to compare cytokeratin protein levels between the METTL3 and EV groups. Scale bar, 100 μm. $^{*}p<0.05$, $^{**}p<0.01$, $^{***}p<0.001$, $^{****}p<0.0001$

than the empty vector group (Figure 3C, D). METTL3-overexpressing nude mice also had a greater number of cytokeratin-positive tumor cells (Figure 3E). The positive rate of popliteal lymph nodes was significantly higher in the SiHa-METTL3 group (100%) than the SiHa-EV group (17%; Figure 3E). In summary, METTL3 overexpression promoted cervical cancer cell metastasis in vivo.

3.4 | *CTSL* is a downstream target gene of METTL3

To identify the downstream target and underlying mechanisms by which METTL3 affects cervical cancer metastasis, we undertook MeRIP sequencing (MeRIP-seq) analysis of METTL3-knockdown (siMETTL3#1) and normal control (siNC) CaSki cells to detect differences in m6A modification. Additionally, the samples were analyzed by RNA sequencing (RNA-seq) to identify differentially expressed genes (DEGs). Association analysis was carried out on MeRIP-seq and RNA-seq data to determine the influence of the m6A modification on differential gene expression. Gene Ontology analysis of RNA-seq data showed that METTL3 was related to ECM organization and cell migration, motility, and adhesion (Figure 4A). Moreover, Kyoto Encyclopedia of Genes and Genomes pathway analysis showed that METTL3 knockdown in cervical cancer cells resulted in a significant change in the ECM receptor and Wnt signaling pathways (Figure 4B). Thus, METTL3 has a potential function in regulating cervical cancer metastasis. Next, we compared the DEGs identified by RNA-seq and the related genes identified by MeRIP-seq using a Venn diagram, which revealed 916 DEGs in common between the two analyses (Figure 4C). To identify possible downstream target genes of METTL3, we analyzed these 916 common genes and 84 human tumor metastasis-related genes[28] using a Venn diagram and found 15 genes in common (Figure 4D). The m6A modification could affect mRNA stability and translation. Therefore, there was a potential trend in the expression levels of genes commonly up- or downregulated in both assays or upregulated in one assay and downregulated in the other assay. The 15 common genes were labeled in the nine-quadrant diagram of the co-regulation relationship between the two assays. The expression levels of four of these genes, *CD44*, *CTSL*, plasminogen activator urokinase receptor (*PLAUR*), and vascular endothelial growth factor receptor (*VEGFR*), were positively correlated with METTL3 levels in both assays (Figure 4E). Of these four genes, only *CTSL* showed significantly decreased expression levels in METTL3-knockdown cervical cancer cells (Figures 4F and S1B,C). As expected, *CTSL* mRNA levels were higher in METTL3-overexpressing cervical cancer cells than in control cells (Figures 4G and S1B,C). These results were verified by examining protein expression levels (Figures 4H and S1A), which confirmed that METTL3 regulated CTSL expression in cervical cancer cell lines. Furthermore, IHC analysis of CTSL and METTL3 expression levels in 143 cervical cancer tissue samples from our center showed a positive correlation between CTSL and METTL3 expression levels (Figure 4I).

To further determine whether *CTSL* is a key downstream target of METTL3, we undertook a rescue assay. We first knocked down CTSL in CaSki and SiHa cells (Figure 5A) and verified that CTSL promoted cervical cancer cell migration and invasion (Figure 5B–E). We then knocked down CTSL in SiHa cells stably overexpressing METTL3, and overexpressed CTSL in CaSki cells with METTL3 knocked down (Figure 5F). As expected, CTSL deficiency in METTL3-overexpressing cervical cancer cells led to decreased cell migration and invasion (Figure 5I,J). Consistently, CTSL overexpression reversed the inhibition of cervical cancer cell metastasis by METTL3 knockdown (Figure 5G,H). In conclusion, *CTSL* is the downstream target of METTL3, and METTL3 promotes cervical cancer cell metastasis by regulating CTSL expression.

3.5 | *CTSL* is regulated by METTL3 in an m6A-dependent manner

The MeRIP-seq results indicated that METTL3 knockdown significantly repressed m6A levels in cervical cancer cells (Figure 6A). A schematic diagram revealed an m6A region in the 5′-UTR of *CTSL* mRNA, and its peak (named 9306) abundance was significantly lower in METTL3-knockdown cells than control cells (Figure 6B). The RIP-qPCR analysis showed strong binding of METTL3 with *CTSL* (Figure 6C). The MeRIP-qPCR analysis showed that METTL3 knockdown decreased the m6A modification levels of *CTSL* mRNA, whereas METTL3 overexpression increased these levels (Figure 6D). Furthermore, MeRIP-qPCR analysis of the 9306 region confirmed the MeRIP-seq results. METTL3 knockdown decreased, while METTL3 overexpression increased, m6A modification levels in the 9306 region (Figure 6E). To further determine the specificity of METTL3-mediated *CTSL* methylation, we knocked down METTL14 and RBM15 in CaSki and SiHa cells (Figure S2A–D), and MeRIP-qPCR showed that METTL14 or RBM15 knockdown did not significantly affect the m6A modification levels of *CTSL* mRNA in cervical cancer cells (Figure S2E,F). Meanwhile, plasmids encoding the WT and mutated 9306 region were transfected into cervical cancer cells. The m6A modification levels of *CTSL* mRNA were significantly downregulated after mutating the 9306 region in *CTSL* mRNA (Figure 6F). Transwell

FIGURE 4 *CTSL* is a downstream target gene of methyltransferase-like 3 (METTL3). (A,B) Methylated RNA immunoprecipitation sequencing (MeRIP-seq) and RNA sequencing (RNA-seq) were carried out for METTL3-knockdown (siMETTL3#1) and control (siNC) CaSki cells. Gene Ontology (GO) function enrichment and Kyoto Encyclopedia of Genes and Genomes (KEGG) pathway enrichment analysis were undertaken for genes with significant differences in expression levels between the two groups, as determined by RNA-seq. (C–E) Differentially expressed genes identified by RNA-seq and peak-related genes identified by MeRIP-seq were analyzed using Venn diagrams and reanalyzed with 84 tumor metastasis-related genes. Fifteen common metastasis-related genes were identified and labeled in the nine-quadrant graph of the co-modulation relationship between the RNA-seq and MeRIP-seq data. Significant differences were identified. *CD44*, *PLAUR*, *VEGFR*, and *CTSL* expression levels were positively correlated with METTL3 levels in RNA-seq and MeRIP-seq data. (F,G) Expression levels of *CD44*, *PLAUR*, *VEGFR*, and *CTSL* genes in METTL3-knockdown and control CaSki cells were determined by RT-quantitative PCR and verified in METTL3-overexpressing SiHa cells. (H) Western blot analysis was used to determine cathepsin L (CTSL) protein levels in cervical cancer cells after METTL3 knockdown/overexpression. (I) Relationship between METTL3 and CTSL levels determined in 143 cervical cancer tissues by immunohistochemistry. $^{*}p<0.05$, $^{**}p<0.01$, $^{***}p<0.001$, $^{****}p<0.0001$

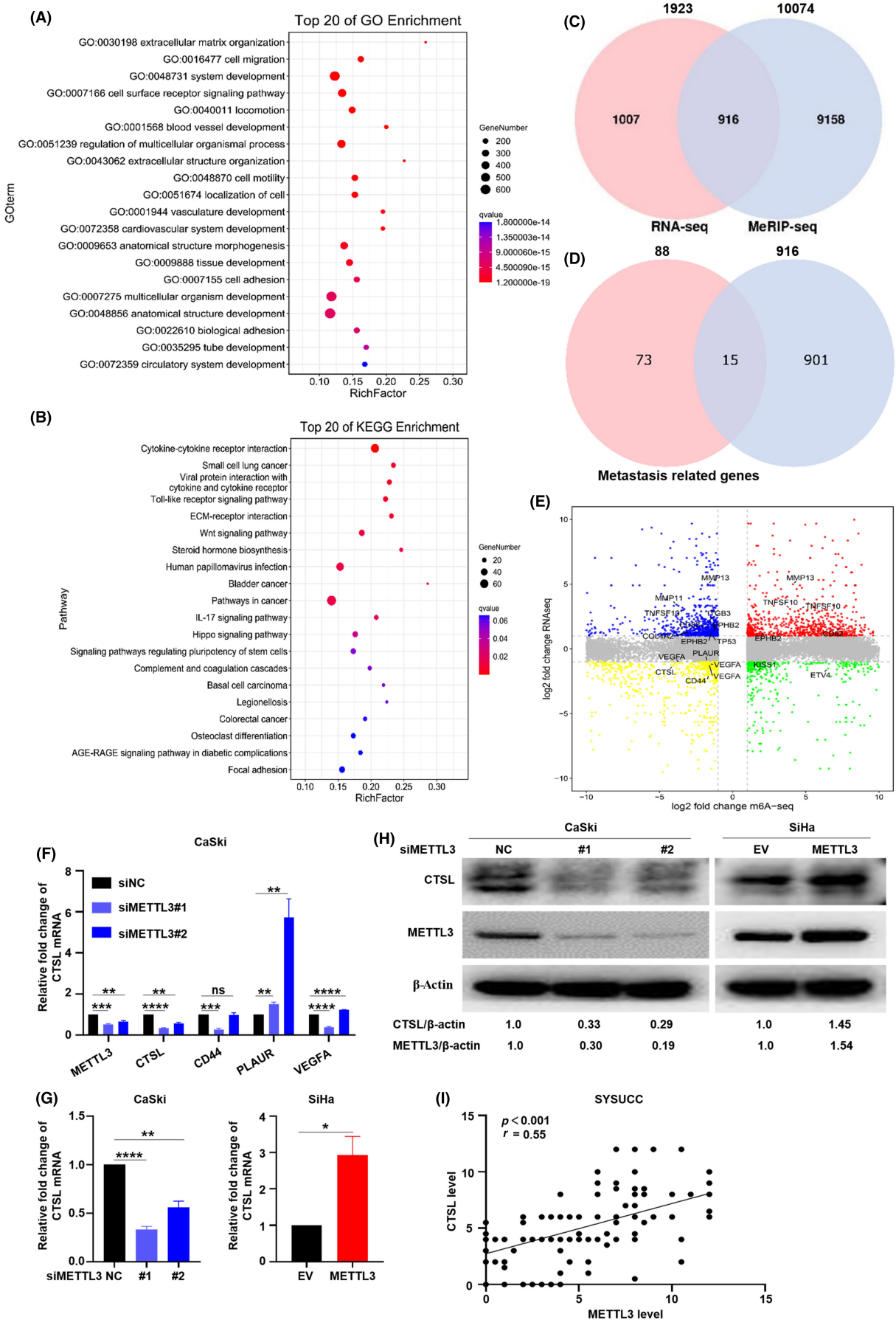
(A)
Top 20 of GO Enrichment
GO:0030198 extracellular matrix organization
GO:0016477 cell migration
GO:0048731 system development
GO:0007166 cell surface receptor signaling pathway
GO:0040011 locomotion
GO:0001568 blood vessel development
GO:0051239 regulation of multicellular organismal process
GO:0043062 extracellular structure organization
GO:0048870 cell motility
GO:0051674 localization of cell
GO:0001944 vasculature development
GO:0072358 cardiovascular system development
GO:0009653 anatomical structure morphogenesis
GO:0009888 tissue development
GO:0007155 cell adhesion
GO:0007275 multicellular organism development
GO:0048856 anatomical structure development
GO:0022610 biological adhesion
GO:0035295 tube development
GO:0072359 circulatory system development
GOterm
RichFactor
GeneNumber
200
300
400
500
600
qvalue
1.800000e-14
1.350003e-14
9.000060e-15
4.500090e-15
1.200000e-19
(B)
Top 20 of KEGG Enrichment
Cytokine-cytokine receptor interaction
Small cell lung cancer
Viral protein interaction with cytokine and cytokine receptor
Toll-like receptor signaling pathway
ECM-receptor interaction
Wnt signaling pathway
Steroid hormone biosynthesis
Human papillomavirus infection
Bladder cancer
Pathways in cancer
IL-17 signaling pathway
Hippo signaling pathway
Signaling pathways regulating pluripotency of stem cells
Complement and coagulation cascades
Basal cell carcinoma
Legionellosis
Colorectal cancer
Osteoclast differentiation
AGE-RAGE signaling pathway in diabetic complications
Focal adhesion
Pathway
RichFactor
GeneNumber
20
40
60
qvalue
0.06
0.04
0.02
(C)
1923
10074
1007
916
9158
RNA-seq
MeRIP-seq
(D)
88
916
73
15
901
Metastasis related genes
(E)
log2 fold change RNAseq
log2 fold change m6A-seq
MMP13
MMP11
TNFSF10
TNFSF18
ITGB3
EPHB2
COL4A2
TP53
VEGFA
PLAUR
CTSL
CD44
KIS91
ETV4
(F)
CaSki
siNC
siMETTL3#1
siMETTL3#2
Relative fold change of CTSL mRNA
METTL3
CTSL
CD44
PLAUR
VEGFA
(H)
CaSki
SiHa
siMETTL3
NC
#1
#2
EV
METTL3
CTSL
METTL3
β-Actin
CTSL/β-actin 1.0 0.33 0.29 1.0 1.45
METTL3/β-actin 1.0 0.30 0.19 1.0 1.54
(G)
CaSki
SiHa
Relative fold change of CTSL mRNA
siMETTL3 NC #1 #2
EV METTL3
(I)
SYSUCC
p < 0.001
r = 0.55
CTSL level
METTL3 level

cell migration and invasion experiments showed that the 9306 WT plasmid promoted cervical cancer cell metastasis, but the mutant plasmid had no effect (Figure 6G–J). Our results revealed the important role of the m6A modification of *CTSL* mRNA in promoting cervical cancer metastasis. We further found that the m6A modification levels of *CTSL* mRNA were significantly upregulated in cervical cancer cells compared with NCECs, suggesting that the m6A modification of *CTSL* mRNA promoted the occurrence of cervical cancer (Figure 6K). Thus, *CTSL* is regulated by METTL3 in an m6A-dependent manner.

3.6 | IGF2BP2 mediates METTL3-regulated stability of *CTSL* mRNA

After the methyltransferase-catalyzed m6A modification, RNA recognition proteins (known as readers) are required to read the methylation information and participate in downstream RNA regulation. Studies have reported that the IGF2BP family is involved in increasing mRNA stability.[29] Radioimmunoprecipitation-qPCR was used to identify the m6A readers of *CTSL* transcripts. We found that IGF2BP2 specifically bound to *CTSL* mRNA in SiHa cells (Figure 7A) and CaSki cells (Figure 7B). Knockdown of IGF2BP2 (Figure 7C) was then shown to inhibit cervical cancer cell migration (Figure 7D,E), indicating that IGF2BP2 also plays an oncogenic role in cervical cancer cell metastasis. To further elucidate the interaction between IGF2BP2 and *CTSL* mRNA, we designed WT and mutant probes of the *CTSL* 9306 region. An RNA pull-down experiment showed that IGF2BP2 protein bound to the *CTSL* 9306 region WT probe; however, this binding was significantly inhibited when the *CTSL* 9306 region was mutated (Figure 7F). In addition, the interaction between IGF2BP2 and *CTSL* mRNA decreased after METTL3 knockdown and increased after METTL3 overexpression (Figure 7G). An RNA stability assay showed that the half-life of *CTSL* mRNA was shorter in METTL3-knockdown and IGF2BP2-silenced cells than in control cells (Figure 7H,I). METTL3 overexpression promoted CTSL expression, but these effects were attenuated by simultaneous IGF2BP2 knockdown (Figure 7J). Taken together, these results confirmed that methylated *CTSL* mRNA was recognized by IGF2BP2, and METTL3/IGF2BP2 enhanced *CTSL* mRNA stability.

4 | DISCUSSION

Cervical cancer is the most common gynecological malignancy in China.[2] Tumor recurrence and metastasis remain the main causes of cervical cancer treatment failure. Investigation of the mechanisms underlying cervical cancer metastasis and the development of novel therapeutic targets are urgently needed. Recent studies have shown that the abnormal expression of m6A regulators plays an important role in cervical cancer progression.[24,30–32] However, few studies have investigated the role of METTL3 in cervical cancer metastasis. We first demonstrated the role of the METTL3-IGF2BP2-CTSL signaling axis in cervical cancer metastasis. Higher levels of METTL3, a key component of the N6-methyltransferase complex, were associated with poorer prognosis in cervical cancer patients. We found that METTL3 promoted cervical cancer metastasis in vitro and in vivo. By integrating DEGs identified by RNA-seq and MeRIP-seq, we showed that *CTSL* was the target gene of METTL3. METTL3 promoted tumor metastasis by binding to the 5′-UTR of *CTSL* mRNA and promoting its expression. Furthermore, methylated *CTSL* mRNA was recognized by the m6A reader IGF2BP2, which bound to *CTSL* mRNA and enhanced its stability. Overall, our study identified a novel epigenetic mechanism for the pathogenesis of cervical cancer. METTL3 was shown to be a potential prognostics marker and therapeutic target for cervical cancer.

A major protein in the m6A methyltransferase complex, METTL3 plays important roles in many malignancies.[33,34] Our study revealed that METTL3 acts as an oncogene during cervical cancer metastasis in vitro and in vivo, which is consistent with previously reported findings. For example, METTL3 has been reported to promote hepatocellular carcinoma cell metastasis by mediating the m6A-induced translation of *SNAIL* mRNA.[34] METTL3 also plays a vital oncogenic role in colorectal cancer metastasis by maintaining SOX2 expression through an m6A-IGF2BP2-dependent mechanism.[20] However, other studies have reported conflicting results. For example, in glioblastoma stem cells, METTL3 acts as a tumor suppressor.[23] METTL3 has also been shown to inhibit endometrial tumorigenesis.[21] Thus, it is necessary to study the specific role of METTL3 in the cancer type of interest. We found an oncogenic role of METTL3 in promoting cervical cancer metastasis, indicating the broad effects of METTL3 and m6A methylation on cervical cancer development and their important in the development of precision therapies.

In vivo studies have indicated that METTL3 is related to lung metastasis in gastric cancer,[35] papillary thyroid,[36] esophageal,[37] and liver cancer.[15] However, studies on METTL3 and lymph node metastasis in vivo have rarely been reported. We established a tail vein lung metastasis model and a popliteal lymph node metastasis model in nude mice and found that METTL3 contributed to the formation

FIGURE 5 Methyltransferase-like 3 (METTL3) promotes cervical cancer cell metastasis in a cathepsin L (CTSL)-dependent manner. (A). Western blot analysis was used to determine cathepsin L (CTSL)-knockdown efficiency (siCTSL#1, siCTSL#2). (B–E) Images and quantification of Transwell migration and invasion assays of CTSL-knockdown versus normal control (NC) cells. Scale bar, 100 μm. (F) Western blotting of METTL3 and CTSL protein in SiHa cells transfected with empty vector (EV), METTL3-overexpression vector, siCTSL#1, and METTL3-overexpression vector +siCTSL#1 (left); western blotting of METTL3 and CTSL protein in CaSki cells transfected with siNC, siMETTL3#1, CTSL-overexpression vector, and siMETTL3#1 + CTSL-overexpression vector (right). Images and quantification of migrated and invasive CaSki (G,H) and SiHa (I,J) cells. Scale bar, 100 μm. $^{*}p < 0.05$, $^{**}p < 0.01$, $^{***}p < 0.001$, $^{****}p < 0.0001$

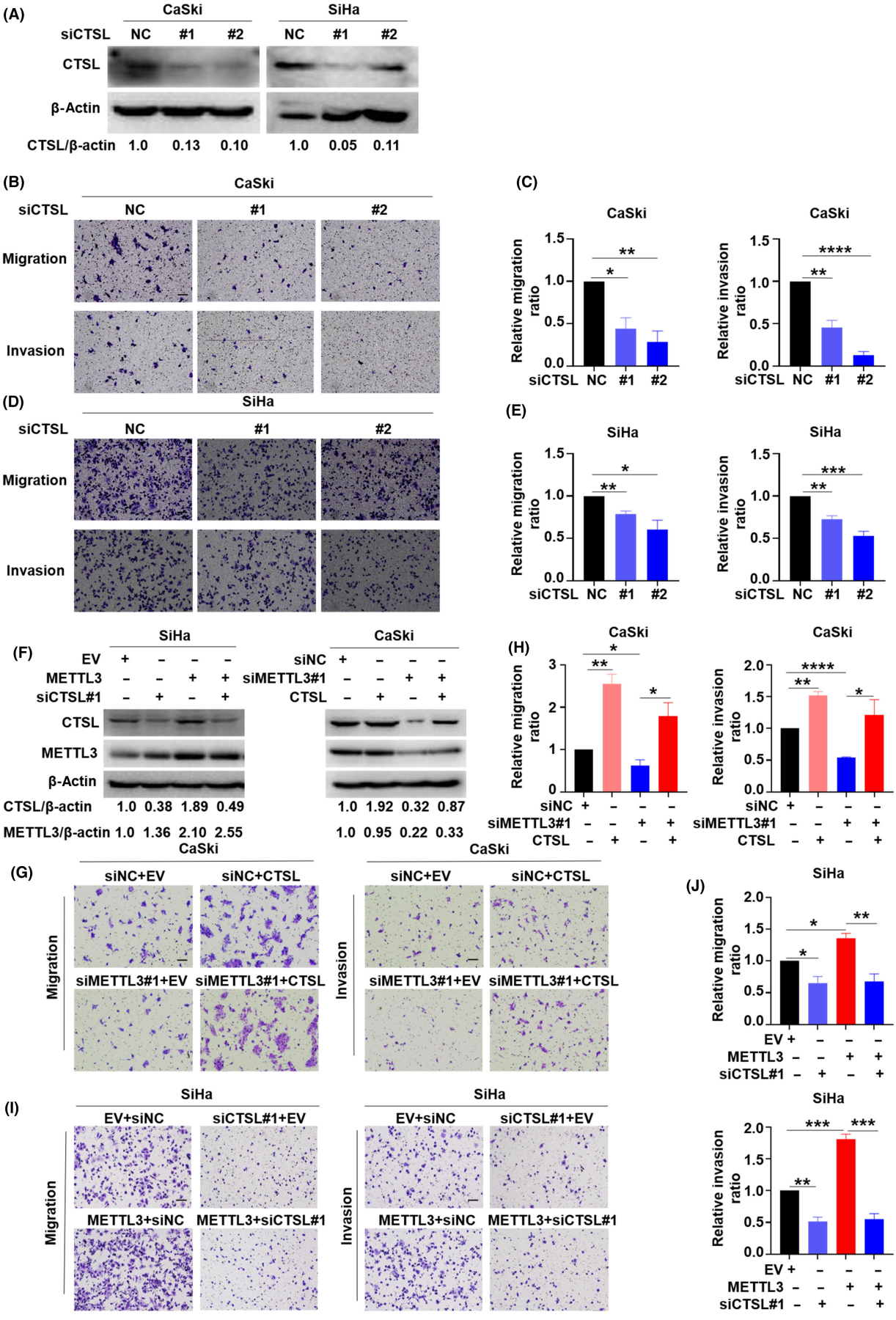
(A)
CaSki
SiHa
siCTSL NC #1 #2 NC #1 #2
CTSL
β-Actin
CTSL/β-actin 1.0 0.13 0.10 1.0 0.05 0.11
(B)
CaSki
siCTSL NC #1 #2
Migration
Invasion
(C)
CaSki
Relative migration ratio
Relative invasion ratio
siCTSL NC #1 #2
(D)
SiHa
siCTSL NC #1 #2
Migration
Invasion
(E)
SiHa
Relative migration ratio
Relative invasion ratio
siCTSL NC #1 #2
(F)
SiHa
EV
METTL3
siCTSL#1
CTSL
METTL3
β-Actin
CTSL/β-actin 1.0 0.38 1.89 0.49
METTL3/β-actin 1.0 1.36 2.10 2.55
CaSki
siNC
siMETTL3#1
CTSL
1.0 1.92 0.32 0.87
1.0 0.95 0.22 0.33
(H)
CaSki
Relative migration ratio
Relative invasion ratio
siNC
siMETTL3#1
CTSL
(G)
CaSki
siNC+EV
siNC+CTSL
siMETTL3#1+EV
siMETTL3#1+CTSL
Migration
Invasion
(J)
SiHa
Relative migration ratio
Relative invasion ratio
EV
METTL3
siCTSL#1
(I)
SiHa
EV+siNC
siCTSL#1+EV
METTL3+siNC
METTL3+siCTSL#1
Migration
Invasion

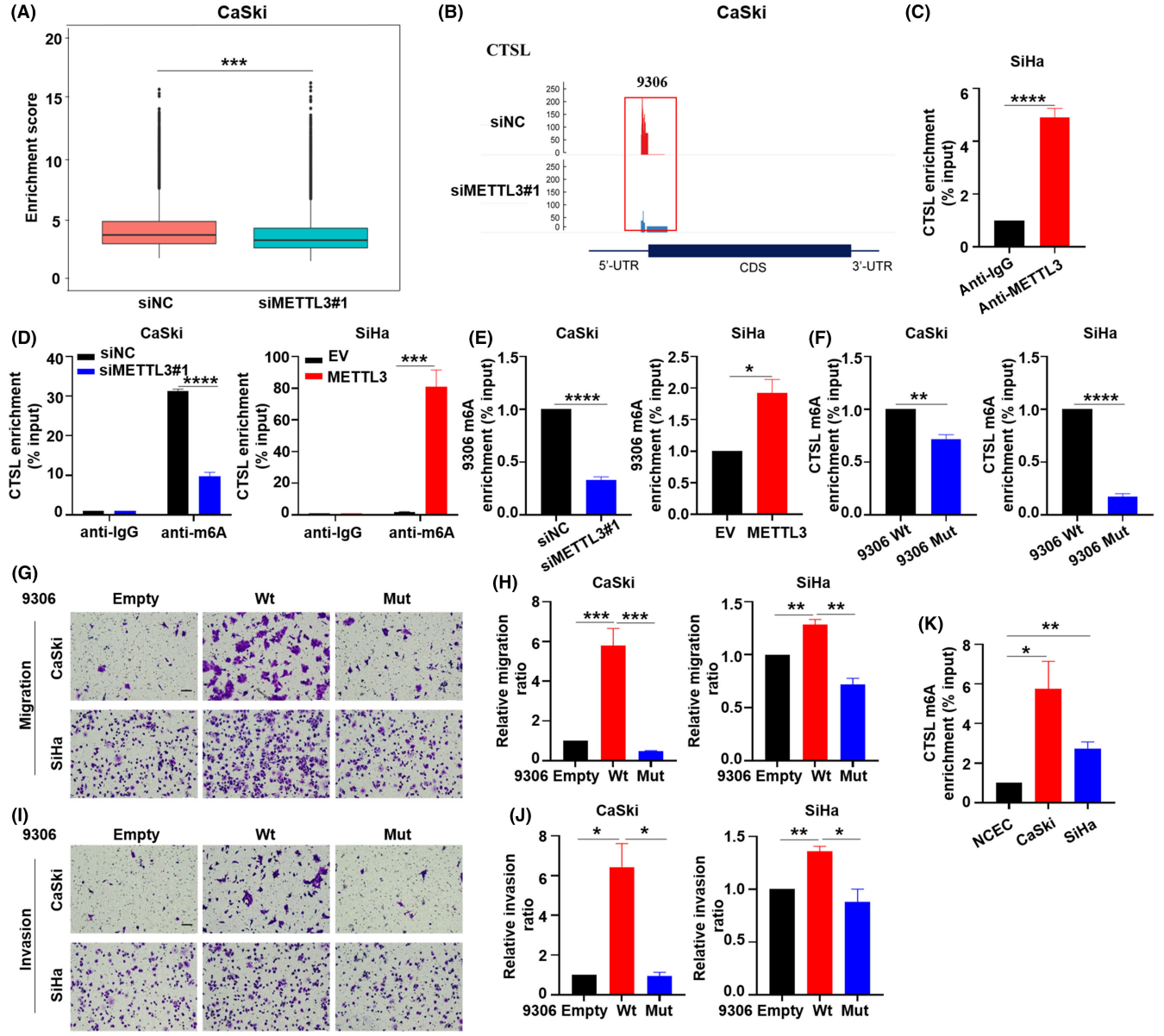

FIGURE 6 Cathepsin L (CTSL) is regulated by methyltransferase-like 3 (METTL3) in an N6-methyladenosine (m6A)-dependent manner. (A) Methylated RNA immunoprecipitation sequencing (MeRIP-seq) revealed the m6A modification levels of normal control (siNC)- and siMETTL3#1-transfected CaSki cells. (B) MeRIP-seq results revealed an m6A modification region (9306) in *CTSL* mRNA, and the modification peak decreased significantly after METTL3 knockdown. (C) RIP-quantitative PCR showed the binding of METTL3 and *CTSL*. (D,E) MeRIP-quantitative PCR (qPCR) was used to assess m6A modification levels in the *CTSL* mRNA and its 9306 region after METTL3 knockdown or overexpression. (F–J) CaSki and SiHa cells were transfected with a plasmid encoding WT or mutant *CTSL* mRNA 9306 regions, and m6A modification levels of *CTSL* mRNA were detected by MeRIP-qPCR. Transwell cell migration and invasion experiments were carried out. Scale bar, 100 μm. (K) m6A modification levels of *CTSL* mRNA in normal cervical epithelial cells and cervical cancer cells were detected by MeRIP-qPCR. $^{*}p<0.05$, $^{**}p<0.01$, $^{***}p<0.001$, $^{****}p<0.0001$

FIGURE 7 Insulin-like growth factor 2 mRNA-binding protein 2 (IGF2BP2) specifically binds to cathepsin L (*CTSL*) transcripts. (A) RIP-quantitative PCR (qPCR) indicated *CTSL* mRNA enrichment in anti-IGF2BP1, -IGF2BP2, and -IGF2BP3 Ab precipitates from SiHa cells. (B) RIP-qPCR indicated the *CTSL* mRNA was precipitated by the anti-IGF2BP2 Ab in CaSki cells. (C–E) CaSki and SiHa cells were transfected with IGF2BP2 (siIGF2BP2#1, siIGF2BP2#2) or negative control (siNC) siRNAs, and Transwell cell migration assays were carried out. Scale bar, 100 μm. (F) RNA pulldown assay showing the binding of IGF2BP2 to the WT and mutant *CTSL* mRNA 9306-region probes in CaSki and SiHa cells. (G) RIP-qPCR indicated *CTSL* mRNA levels in anti-IGF2BP2 Ab precipitates after methyltransferase-like 3 (METTL3) knockdown and overexpression. (H,I) *CTSL* mRNA decay rate in METTL3-knockdown and IGF2BP2-silenced cells after actinomycin D (Act D, 10 μg/ml) treatment. (J) Western blotting of CTSL, METTL3, and IGF2BP2 proteins in SiHa cells transfected with empty vector (EV), METTL3-overexpression vector (METTL3) and IGF2BP2 siRNA, or both. $^{*}p<0.05$, $^{**}p<0.01$, $^{***}p<0.001$, $^{****}p<0.0001$

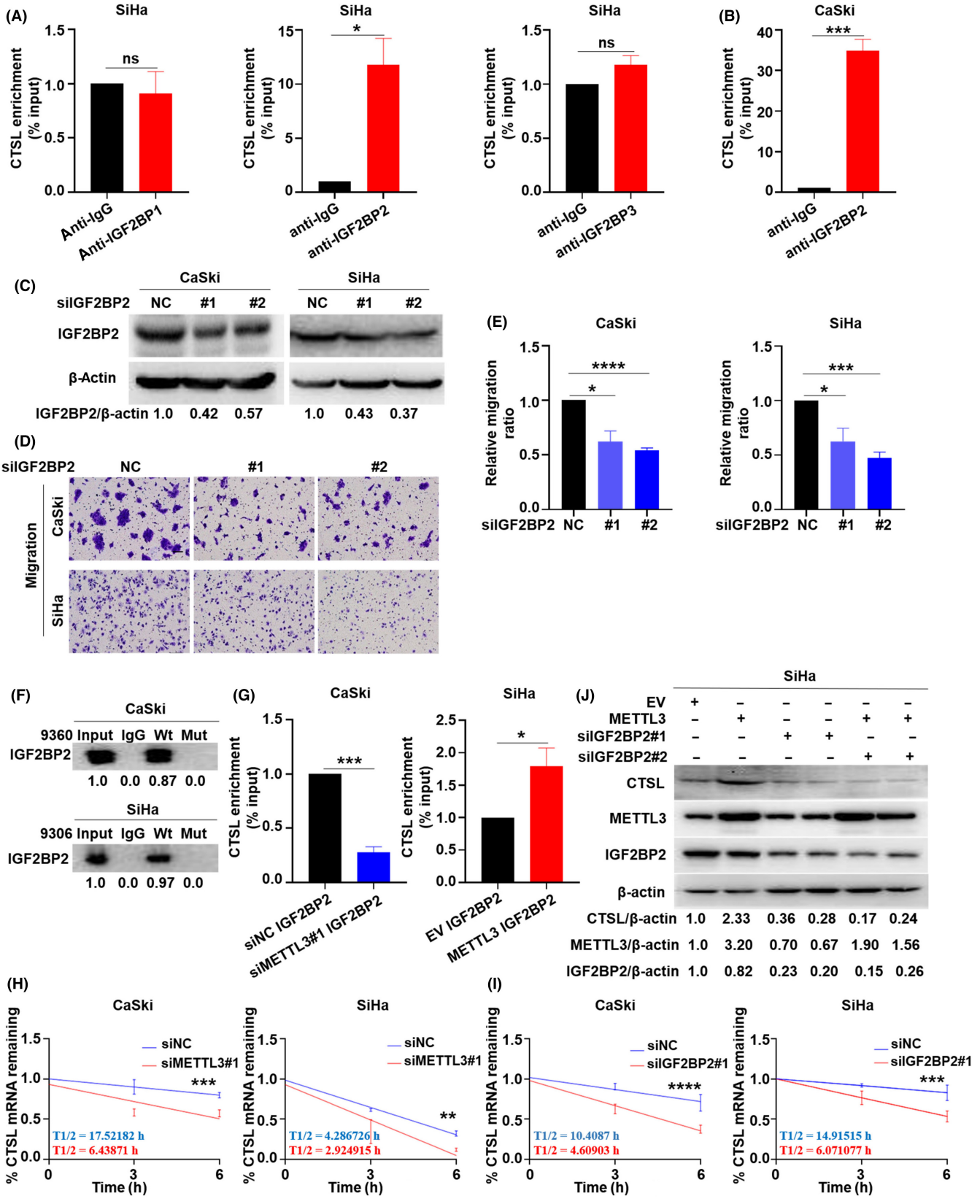

of metastatic cervical cancer foci in both models, indicating a previously unrecognized role of METTL3 in the lymph node metastasis of cervical cancer.

A major member of the lysosomal cysteine protease family, CTSL is upregulated in various cancers and plays an important role in promoting tumor cell metastasis.[38–44] Acute exposure to

hypoxic or acidic conditions, *CTSL* promotor hypomethylation, gene amplification, and increased promotor activity have been shown to upregulate CTSL expression.[45–49] However, whether CTSL expression is regulated by RNA modification remains unknown. Moreover, the regulatory mechanism of CTSL in cervical cancer is unclear. We discovered a new epigenetic modulation of *CTSL*. We found that METTL3 upregulates CTSL expression, confirmed the oncogenic effect of CTSL, and revealed an m6A-depedent regulatory mechanism of CTSL in cervical cancer. The m6A modification is enriched in the 5′-UTR, coding sequence, and 3′-UTR of transcripts.[50] Our data revealed several m6A sites in the 5′-UTR of *CTSL* mRNA, and these positively regulated *CTSL* mRNA stability by binding with IGF2BP2. Consistent with these findings, the m6A-modification of the 5′-UTR of *PDK4* mRNA has been shown to increase its half-life in an IGF2BP3-dependent manner.[51]

RNA recognition proteins include the YTH domain-containing and IGF2BP protein families.[27,52,53] The m6A readers are involved in controlling mRNA fate, and in contrast to YTHDF2-mediated mRNA decay, IGF2BP proteins preferentially recognize m6A-modified mRNAs and promote their stability.[53] We first found that IGF2BP2 directly bound to the m6A sites in the *CTSL* 5′-UTR and enhanced *CTSL* mRNA stability in an m6A-dependent manner. Previous studies have shown that increased IGF2BP2 expression levels promote the metastasis of oral squamous cell carcinoma[54] and gastric cancer.[55] Here, we revealed the oncogenic role of IGF2BP2 in cervical cancer metastasis and its regulatory effect on *CTSL* mRNA stability to enhance cervical cancer progression. Our results could partially explain the role of IGF2BP2 in preserving the cervical cancer metastasis phenotype.

These findings indicate a new underlying mechanism of METTL3 in cervical cancer metastasis. However, this study has some limitations. The reason METTL3 is upregulated in cervical cancer tissues remains unclear. In our future work, we will investigate the molecular mechanism of METTL3 upregulation. The function of the m6A modification of RNA in tumor progression is complicated, and thus, more research is required to increase our understanding of its role in tumorigenesis.

We identified an oncogene role of METTL3 in cervical cancer metastasis. *CTSL* is the direct target gene of METTL3 and is regulated through a METTL3-IGF2BP2-m6A-dependent mechanism. We revealed a novel mechanism by which METTL3 regulates cervical cancer metastasis, suggesting that METTL3 is an important predictor of cervical cancer metastasis.

ACKNOWLEDGMENTS

We thank Professor Limin Zheng from the School of Life Sciences at Sun Yat-sen University for providing us with the experimental platform and Professor Jianhong Fang from the School of Life Sciences at Sun Yat-sen University for essential technical assistance and suggestions for the study conception.

FUNDING INFORMATION

This work was supported by a grant from the Natural Science Foundation of China (grant number 81872434).

CONFLICT OF INTEREST

The authors declare no conflict of interest.

ETHICS STATEMENT

The present study was performed according to the ethical standards of the World Medical Association Declaration of Helsinki and was approved by the Institutional Review Board and Independent Ethics Committee of the Sun Yat-sen University Cancer Center (B2021-384-01). The requirement for informed consent was waived because the data used in this study were obtained from previous clinical records and will not adversely affect the rights or health of the subject. We declare that we will protect the confidentiality of the personal information of research subjects. All animal experiments were performed in accordance with the protocol approved by our institutional animal care committee (L102042021010C).

ORCID

Min Zheng https://orcid.org/0000-0002-0329-9680

REFERENCES

1. Bray F, Ferlay J, Soerjomataram I, Siegel R, Torre L, Jemal A. Global cancer statistics 2018: GLOBOCAN estimates of incidence and mortality worldwide for 36 cancers in 185 countries. *CA Cancer J Clin*. 2018;68(6):394-424.
2. Zheng RS, Zeng HM, Wang SM, et al. Cancer incidence and mortality in China, 2016. *JNCC*. 2022;2(1):1-9.
3. Shin S, Lee G, Lee M, et al. Aberrant expression of CITED2 promotes prostate cancer metastasis by activating the nucleolin-AKT pathway. *Nat Commun*. 2018;9(1):4113.
4. Singh R, Karri D, Shen H, et al. TRAF4-mediated ubiquitination of NGF receptor TrkA regulates prostate cancer metastasis. *J Clin Invest*. 2018;128(7):3129-3143.
5. Yuan H, Han Y, Wang X, et al. SETD2 restricts prostate cancer metastasis by integrating EZH2 and AMPK signaling pathways. *Cancer Cell*. 2020;38(3):350-365.
6. Zhang X, Jia G. RNA epigenetic modification: N6-methyladenosine. *Yi chuan = Hereditas*. 2016;38(4):275-288.
7. Visvanathan A, Somasundaram K. mRNA traffic control reviewed: N6-Methyladenosine (m6A) takes the driver's seat bioessays. *News Rev Mol Cell Develop Biol*. 2018;40(1):1700093.
8. Alarcón C, Lee H, Goodarzi H, Halberg N, Tavazoie S. N6-methyladenosine marks primary microRNAs for processing. *Nature*. 2015;519(7544):482-485.
9. He L, Li H, Wu A, Peng Y, Shu G, Yin G. Functions of N6-methyladenosine and its role in cancer. *Mol Cancer*. 2019;18(1):176.
10. Yang Y, Hsu P, Chen Y, Yang Y. Dynamic transcriptomic mA decoration: writers, erasers, readers and functions in RNA metabolism. *Cell Res*. 2018;28(6):616-624.
11. Wei W, Ji X, Guo X, Ji S. Regulatory role of N -methyladenosine (mA) methylation in RNA processing and human diseases. *J Cell Biochem*. 2017;118(9):2534-2543.

12. Batista P, The RNA. Modification N-methyladenosine and its implications in human disease. *Genom Proteomic Bioinform*. 2017;15(3):154-163.
13. Barbieri I, Tzelepis K, Pandolfini L, et al. Promoter-bound METTL3 maintains myeloid leukaemia by mA-dependent translation control. *Nature*. 2017;552(7683):126-131.
14. Vu L, Pickering B, Cheng Y, et al. The N-methyladenosine (mA)-forming enzyme METTL3 controls myeloid differentiation of normal hematopoietic and leukemia cells. *Nat Med*. 2017;23(11):1369-1376.
15. Chen M, Wei L, Law C, et al. RNA N6-methyladenosine methyltransferase-like 3 promotes liver cancer progression through YTHDF2-dependent posttranscriptional silencing of SOCS2. *Hepatology*. 2018;67(6):2254-2270.
16. Chen Y, Peng C, Chen J, et al. WTAP facilitates progression of hepatocellular carcinoma via m6A-HuR-dependent epigenetic silencing of ETS1. *Mol Cancer*. 2019;18(1):127.
17. Han J, Wang J, Yang X, et al. METTL3 promote tumor proliferation of bladder cancer by accelerating pri-miR221/222 maturation in m6A-dependent manner. *Mol Cancer*. 2019;18(1):110.
18. Jin H, Ying X, Que B, et al. N-methyladenosine modification of ITGA6 mRNA promotes the development and progression of bladder cancer. *EBioMedicine*. 2019;47:195-207.
19. Cheng M, Sheng L, Gao Q, et al. The mA methyltransferase METTL3 promotes bladder cancer progression via AFF4/NF-κB/MYC signaling network. *Oncogene*. 2019;38(19):3667-3680.
20. Li T, Hu P, Zuo Z, et al. METTL3 facilitates tumor progression via an mA-IGF2BP2-dependent mechanism in colorectal carcinoma. *Mol Cancer*. 2019;18(1):112.
21. Liu J, Eckert M, Harada B, et al. mA mRNA methylation regulates AKT activity to promote the proliferation and tumorigenicity of endometrial cancer. *Nat Cell Biol*. 2018;20(9):1074-1083.
22. Li F, Yi Y, Miao Y, et al. N-Methyladenosine modulates nonsense-mediated mRNA decay in human glioblastoma. *Cancer Res*. 2019;79(22):5785-5798.
23. Cui Q, Shi H, Ye P, et al. mA RNA methylation regulates the self-renewal and tumorigenesis of glioblastoma stem cells. *Cell Rep*. 2017;18(11):2622-2634.
24. Wang Q, Guo X, Li L, et al. N-methyladenosine METTL3 promotes cervical cancer tumorigenesis and Warburg effect through YTHDF1/HK2 modification. *Cell Death Dis*. 2020;11(10):911.
25. Zhang L, Huang S, Feng Y, et al. The bidirectional regulation between MYL5 and HIF-1α promotes cervical carcinoma metastasis. *Theranostics*. 2017;7(15):3768-3780.
26. Ratnadiwakara M, Änkö M. mRNA stability assay using transcription inhibition by Actinomycin D in mouse pluripotent stem cells. *Bio-Protocol*. 2018;8(21):e3072.
27. Lan Q, Liu P, Haase J, Bell J, Hüttelmaier S, Liu T. The critical role of RNA mA methylation in cancer. *Cancer Res*. 2019;79(7):1285-1292.
28. Zhu W, Cai M, Tong Z, et al. Overexpression of EIF5A2 promotes colorectal carcinoma cell aggressiveness by upregulating MTA1 through C-myc to induce epithelial-mesenchymaltransition. *Gut*. 2012;61(4):562-575.
29. Deng X, Su R, Weng H, Huang H, Li Z, Chen J. RNA N-methyladenosine modification in cancers: current status and perspectives. *Cell Res*. 2018;28(5):507-517.
30. Wang H, Luo Q, Kang J, et al. YTHDF1 aggravates the progression of cervical cancer through mA-mediated up-regulation of RANBP2. *Front Oncol*. 2021;11:650383.
31. Zou D, Dong L, Li C, Yin Z, Rao S, Zhou Q. The mA eraser FTO facilitates proliferation and migration of human cervical cancer cells. *Cancer Cell Int*. 2019;19:321.
32. Zhou S, Bai Z, Xia D, et al. FTO regulates the chemo-radiotherapy resistance of cervical squamous cell carcinoma (CSCC) by targeting β-catenin through mRNA demethylation. *Mol Carcinog*. 2018;57(5):590-597.
33. Zeng C, Huang W, Li Y, Weng H. Roles of METTL3 in cancer: mechanisms and therapeutic targeting. *J Hematol Oncol*. 2020;13(1):117.
34. Lin X, Chai G, Wu Y, et al. RNA mA methylation regulates the epithelial mesenchymal transition of cancer cells and translation of Snail. *Nat Commun*. 2019;10(1):2065.
35. Zhang H, Qi F, Wang J, et al. The m6A Methyltransferase METTL3-mediated N6-Methyladenosine modification of DEK mRNA to promote gastric cancer cell growth and metastasis. *Int J Mol Sci*. 2022;23(12):6451.
36. Zhu Y, Peng X, Zhou Q, et al. METTL3-mediated m6A modification of STEAP2 mRNA inhibits papillary thyroid cancer progress by blocking the hedgehog signaling pathway and epithelial-to-mesenchymal transition. *Cell Death Dis*. 2022;13(4):358.
37. Liang X, Zhang Z, Wang L, et al. Mechanism of methyltransferase like 3 in epithelial-mesenchymal transition process, invasion, and metastasis in esophageal cancer. *Bioengineered*. 2021;12(2):10023-10036.
38. Pranjol M, Gutowski N, Hannemann M, Whatmore J. The potential role of the proteases Cathepsin D and Cathepsin L in the progression and metastasis of epithelial ovarian cancer. *Biomolecules*. 2015;5(4):3260-3279.
39. Pišlar A, Jewett A, Kos J. Cysteine cathepsins: their biological and molecular significance in cancer stem cells. *Semin Cancer Biol*. 2018;53:168-177.
40. Gocheva V, Joyce J. Cysteine cathepsins and the cutting edge of cancer invasion. *Cell Cycle*. 2007;6(1):60-64.
41. Jedeszko C, Sloane B. Cysteine cathepsins in human cancer. *Biol Chem*. 2004;385(11):1017-1027.
42. Kos J, Stabuc B, Schweiger A, et al. Cathepsins B, H, and L and their inhibitors stefin a and cystatin C in sera of melanoma patients. *Clin Cancer Res*. 1997;3(10):1815-1822.
43. Sudhan D, Siemann D. Cathepsin L targeting in cancer treatment. *Pharmacol Ther*. 2015;155:105-116.
44. Sudhan D, Pampo C, Rice L, Siemann D. Cathepsin L inactivation leads to multimodal inhibition of prostate cancer cell dissemination in a preclinical bone metastasis model. *Int J Cancer*. 2016;138(11):2665-2677.
45. Sudhan D, Siemann D. Cathepsin L inhibition by the small molecule KGP94 suppresses tumor microenvironment enhanced metastasis associated cell functions of prostate and breast cancer cells. *Clin Exp Metastasis*. 2013;30(7):891-902.
46. Cuvier C, Jang A, Hill R. Exposure to hypoxia, glucose starvation and acidosis: effect on invasive capacity of murine tumor cells and correlation with cathepsin (L + B) secretion. *Clin Exp Metastasis*. 1997;15(1):19-25.
47. Samaiya M, Bakhshi S, Shukla A, Kumar L, Chauhan S. Epigenetic regulation of cathepsin L expression in chronic myeloid leukaemia. *J Cell Mol Med*. 2011;15(10):2189-2199.
48. Mao X, Hamoudi R. Molecular and cytogenetic analysis of glioblastoma multiforme. *Cancer Genet Cytogenet*. 2000;122(2):87-92.
49. Jean D, Rousselet N, Frade R. Expression of cathepsin L in human tumor cells is under the control of distinct regulatory mechanisms. *Oncogene*. 2006;25(10):1474-1484.
50. Zhang C, Huang S, Zhuang H, et al. YTHDF2 promotes the liver cancer stem cell phenotype and cancer metastasis by regulating OCT4 expression via m6A RNA methylation. *Oncogene*. 2020;39(23):4507-4518.
51. Li Z, Peng Y, Li J, et al. N-methyladenosine regulates glycolysis of cancer cells through PDK4. *Nat Commun*. 2020;11(1):2578.
52. Wang X, Zhao B, Roundtree I, et al. N(6)-methyladenosine modulates messenger RNA translation efficiency. *Cell*. 2015;161(6):1388-1399.
53. Huang H, Weng H, Sun W, et al. Recognition of RNA N-methyladenosine by IGF2BP proteins enhances mRNA stability and translation. *Nat Cell Biol*. 2018;20(3):285-295.
54. Zhou L, Li H, Cai H, et al. Upregulation of IGF2BP2 promotes Oral squamous cell carcinoma progression that is related to cell

proliferation, metastasis and tumor-infiltrating immune cells. *Front Oncol*. 2022;12:809589.
55. Liu D, Xia A, Wu L, Li S, Zhang K, Chen D. IGF2BP2 promotes gastric cancer progression by regulating the IGF1R-RhoA-ROCK signaling pathway. *Cell Signal*. 2022;94:110313.

SUPPORTING INFORMATION

Additional supporting information can be found online in the Supporting Information section at the end of this article.

How to cite this article: Liu P, Ju M, Zheng X, et al. Methyltransferase-like 3 promotes cervical cancer metastasis by enhancing cathepsin L mRNA stability in an N6-methyladenosine-dependent manner. *Cancer Sci*. 2023;114:837-854. doi:10.1111/cas.15658